Complementary switching in single $Nb_3O_7(OH)$ nanowires

Cite as: APL Mater. 9, 071105 (2021); doi: 10.1063/5.0052589
Submitted: 31 March 2021 • Accepted: 14 June 2021 •
Published Online: 2 July 2021

Carola Ebenhoch,[1] Thomas Gänsler,[2] Stefan Schupp,[1] Matthias Hagner,[1] Anna Frank,[2] Christina Scheu,[2] and Lukas Schmidt-Mende[1,a)]

AFFILIATIONS

[1] Department of Physics, University of Konstanz, 78457 Konstanz, Germany
[2] Max-Planck-Institut für Eisenforschung GmbH, Max-Planck-Straße 1, 40237 Düsseldorf, Germany

[a)] Author to whom correspondence should be addressed: Lukas.Schmidt-mende@uni-konstanz.de

ABSTRACT

Single nanowires and networks are considered as promising candidates for miniaturized memristive devices for brain-inspired systems. Moreover, single crystalline nanostructures are useful model systems to gain a deeper understanding in the involved switching mechanism of the investigated material. Here, we report on hydrothermally grown single crystalline $Nb_3O_7(OH)$ nanowires showing a complementary resistive switching (CRS) behavior. The CRS characteristics can be related to an oxygen vacancy migration at the electrode/metal hydroxide interface. Therefore, an oxygen plasma treatment is used to reduce the oxygen vacancy content, resulting in a total reduction of the device conductivity. Furthermore, temporal resolved current–voltage measurements demonstrate the dependence of the destructive readout process of the resistance states on the voltage amplitude and polarity.

I. INTRODUCTION

Memristive devices are promising candidates for realizing artificial neural networks due to their ability to emulate biological synaptic functions.[1–3] Combined information storage and data processing is achieved by implementing memristive elements in a parallel approach into logic circuits.[4–6] It was shown by Snider in 2008[7] that using a complementary metal-oxide semiconductor (CMOS) combined with a memristive synapse in a crossbar array configuration, neuromorphic computing in a parallel, scalable, and failure-tolerance way is possible. Furthermore, Lu and Lieber[8] summarized possible bottom-up fabrication processes for implementing nanowires or nanobelts in memory based crossbar circuits to increase the device density and allow scaling in three dimensions. However, to solve the sneak path problem in passive crossbar arrays, Linn *et al.*[9] proposed the complementary resistive switching (CRS) by connecting two bipolar memristive elements. Since then, complementary resistive switching (CRS) has also been achieved in memristive devices with only one material type composed of different oxygen-deficient layers.[10] Liu *et al.* studied CRS in niobium oxide-based memory devices by using a bilayer Nb_2O_{5-x}/NbO_y and two electrode configuration in a crossbar array system and could show the absence of the sneak path current.[11] However, CRS devices often show a destructive readout procedure, where the resistance state is overwritten by the readout process.[9] Therefore, additional energy for a write-back step after the readout is necessary to regain the memory state. Approaches to overcome this problem are using unstable, volatile resistive switching devices in a CRS configuration, where the volatile resistive switch is used to readout the second cell.[12] Another solution could be given by using capacitive read-out approaches.[13] However, as the memristive device function strongly depends on the material, its internal structure, defect concentration, and the device architecture,[1,14] detailed analysis of the switching mechanism and neuromorphic behavior is necessary for each device separately. We present in this work a CRS behavior for a single niobium hydroxide [$Nb_3O_7(OH)$] nanowire within a two electrode $Au/Nb_3O_7(OH)/Au$ configuration. The resistance change is related to an oxygen vacancy migration and redistribution. We furthermore demonstrate the temporal behavior of the destructive readout current for different applied potentials. To the best of our knowledge, this is the first report of $Nb_3O_7(OH)$ single nanowires showing a memristive behavior.

II. EXPERIMENTS

The single nanowires are grown in a hydrothermal synthesis approach adapted from Refs. 15 and 16. A synthesis time of 19 h at 200 °C is used. The resulting nanowire powder is dispersed in an ethanol solution by using an ultrasonic bath treatment for 10 min. 5 μl dispersion is dropped on a finger electrode substrate [30 nm gold on top of 10 nm indium doped tin oxide (ITO), 230 nm SiO_2, altogether on top of an *n*-doped (3×10^{17} cm^{-3}) Si wafer], with finger electrode distances of 2.5, 5, 10, and 20 μm, four of each size. For high resolution imaging, a field emission scanning electron microscope (SEM) *Analytic SEM Zeiss Gemini* 500 system is used with an integrated energy dispersive x-ray spectroscopy (EDX) system (0.02–30 keV). For transmission electron microscopy (TEM) characterization, 100 μl dispersion is dropped on a copper TEM sample grid with a lacey carbon support. High resolution imaging and selected area electron diffraction (SAED) are performed on a JEOL JEM-2100Plus operated at 200 kV as well as a C_S image-corrected Thermo Fisher Scientific Titan Themis 80–300 microscope operated at 300 kV. Being optional, an oxygen plasma treatment is done with a *Diener* electronic plasma system (Type: Femto) for 30 s prior to the electronic measurements. Current–voltage characteristics are recorded in vacuum at ~10^{-6} mbar at room temperature by a Keithley 2400 digital multimeter. The Keithley itself is controlled by a self-written Matlab program.

III. RESULTS AND DISCUSSION

TEM analysis of the untreated reaction product (shown in Fig. 1) demonstrates the single crystallinity of the hydrothermally grown nanowires. An average width of 60 nm and a maximum length of 15 μm are observed. Ultrasonic dispersion results in well-separated wires, which enabled further characterization. The nanowires can be observed in two different orientations, along the [001] and [100] axes of the orthorhombic crystal structure. The former, as shown in Fig. 1(b), shows well-defined crystal facets as well as uniform growth in the [010] direction (along the long axis of the wire). The latter [see Fig. 1(c)] reveals the planar stacking faults as observed in Refs. 17–19, which are attributed to oxygen vacancies due to the imperfect stoichiometric nature of the crystal.

Figure 2 shows the device architecture for electronic measurements on single nanowires. The left image shows the finger electrode substrate with a periodic electrode distance. By chance, a single nanowire is found lying on top of two electrodes. On the right, a 3 μm long nanowire contacts two gold electrodes with a distance of 2.5 μm, schematically illustrated in the inset. The device is then implemented in the electronic characterization setup and measured under vacuum.

Typically, the *n*-type semiconducting $Nb_3O_7(OH)$[20,21] nanowire do only show small currents with no visible memristive behavior during the very first measurements. Therefore, an electroforming procedure with 20 V for 300 s is applied, as shown in Fig. 3(a). The gradual increase in the current during electroforming indicates Joule heating. To improve the nanowire/electrode contact, usually an additional preparation step (annealing, oxygen plasma treatment[22,23]) is performed. However, we assume that the contact between the nanowire and the gold electrodes is improved to the Joule heating effect during electroforming and accordingly did not perform another treatment to prevent modifications of $Nb_3O_7(OH)$. Afterward, the devices show a complementary resistive switching behavior [Fig. 3(b)] with a slight asymmetric behavior, which is suggested to result from the asymmetric forming process. The color specifies the cycle number and goes from black to light blue. The current increases upon cycling, whereas a saturation within the first four to five cycles is observed. The curves themselves show a CRS behavior, where increasing the voltage from negative applied bias to positive potentials (solid line) leads to a current increase up to a voltage of ~8 V and drops when going to even higher voltages. It remains in the high resistance state (HRS) when the voltage is decreased again (dashed line). After the polarity change, the device gains back the low resistance state (LRS) again and remains there until ~−15 V is reached. The current drops for even lower voltages again, and the system changes back to its high resistance state. Cycles of only negative/positive polarities, as shown in Figs. 3(c) and 3(d), do not show a memristive behavior. Negative cycling begins at −20 V and is to that point in a low resistance state (LRS).

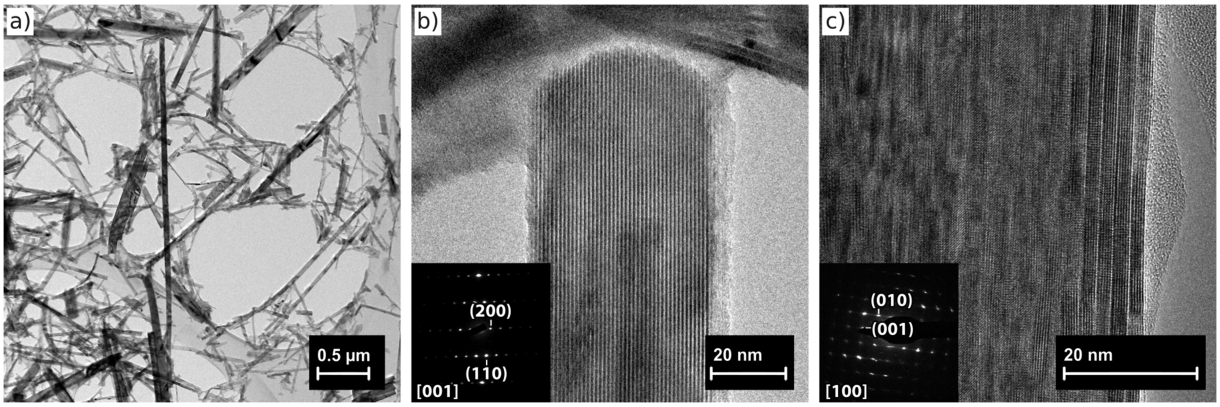

FIG. 1. TEM characterization of the untreated $Nb_3O_7(OH)$ nanowires. (a) Conglomerate of single nanowires and fragments distributed on a carbon support for TEM analysis. (b) Tip of a wire with the optical axis parallel to [001] showing the faceted nature as well as the single crystallinity. Inset: SAED pattern with associated lattice planes. (c) Optical axis parallel to [100] reveals the planar faults in the crystal. Inset: SAED pattern with associated lattice planes.

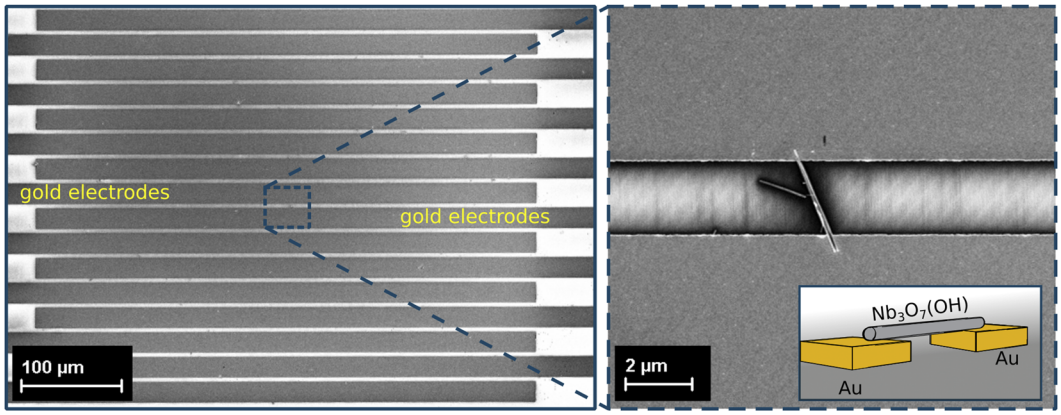

FIG. 2. SEM image of the single nanowire/electrode configuration. (Left) Finger electrode substrate with 2.5 μm distance in between two electrodes. (Right) Single nanowire on top of two gold electrodes with a schematic of the architecture at the bottom right.

After the first cycle, it is found to be in the HRS and remains there for further cycles. For the positive voltage region, the system was already set to the HRS and remains there upon cycling. Therefore, a polarity change is necessary to change the resistance state of the device between low and high resistive states.

Endurance measurements for 1000 cycles are shown in Fig. 4. The inset shows endurance measurements of a second sample. Typically, the switching behavior remains constant for 100 cycles for all devices, whereas afterward, the current either increases, remains constant, or even starts to decrease. However, more statistics in

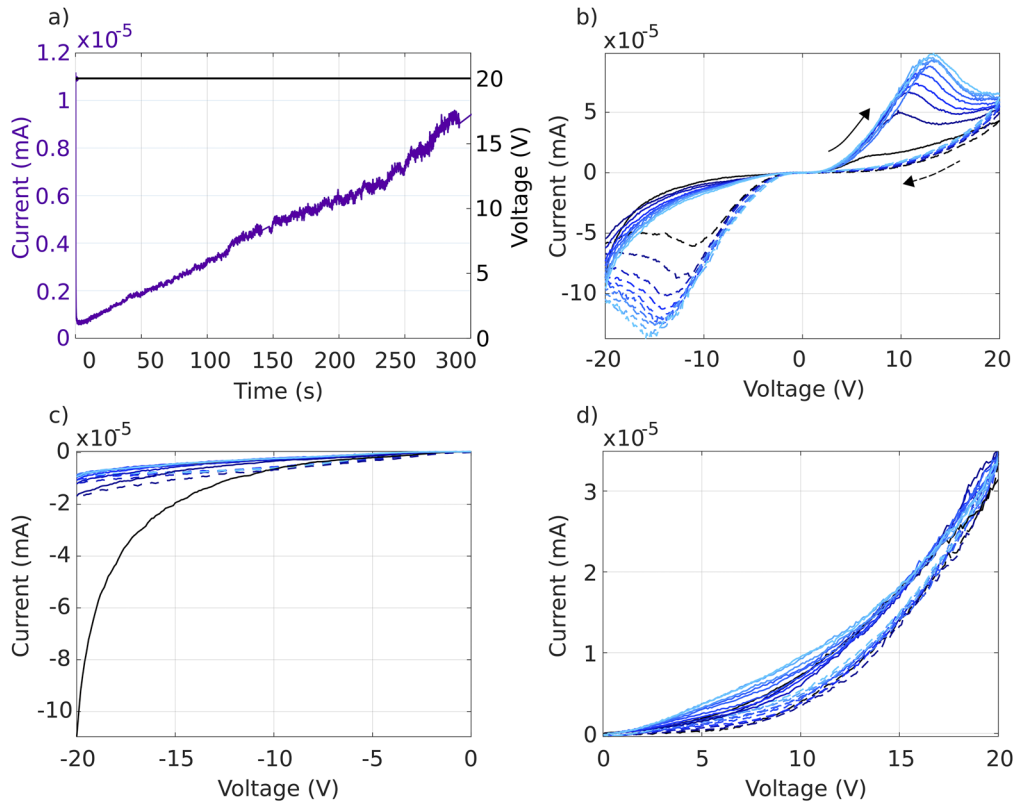

FIG. 3. Electronic characterization of the CRS device. (a) A forming procedure is necessary to set the device into a conductive state. (b) I–V characteristics of the CRS cell. In (c) and (d), cycling with only a negative or positive applied polarity shows no memristive behavior. Time is specified by the color gradient from black to light blue.

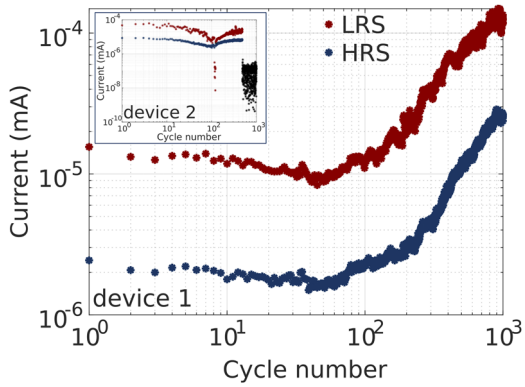

FIG. 4. Endurance measurement for the present CRS cell, which is stable for ~100 cycles. For further cycles, the current increases for the device. The inset shows the endurance of a second device where the current drops, indicating the sample to sample variation for endurance behaviors.

terms of the endurance measurements accompanied by a detailed structural analysis of differently behaving nanowires are necessary to find a suitable explanation for the endurance deviations. Most likely, they are due to an irreversible structural and compositional change.

As a second step, the devices are oxygen plasma treated for 30 s. An oxygen plasma treatment in metal oxides usually leads to a reduction of oxygen vacancies upon diffusion of ionized, radical oxygen species into the material.[24–26] Therefore, the element content is determined by EDX measurements as shown in Fig. SI1. The untreated nanowires show a higher Nb/O ratio, compared to the oxygen plasma treated samples. As oxygen vacancies are electron donor defects, a reduction in the oxygen vacancy concentration upon oxygen plasma treatment results in a lower conductivity of the nanowire. Thereby, the amount of electrons in the conduction band is reduced, which reduces the Fermi energy level. Furthermore, a lower Fermi energy level leads to an increased metal/metal oxide interface barrier.[20,27] Figure 5 shows that the device has lost

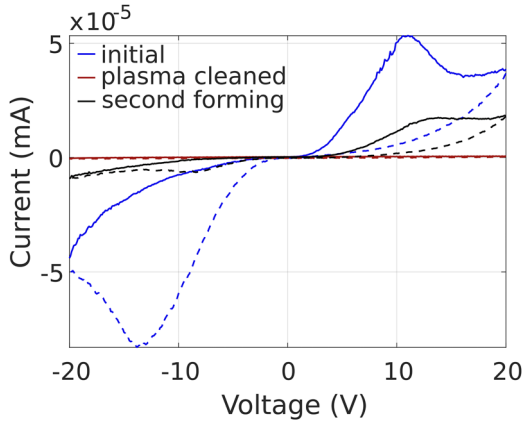

FIG. 5. I–V characteristics for the CRS device in the initial stage and after different treatments. The plasma cleaning leads to vanishing conductivity. After a long electroforming procedure for ~1 h, the behavior does recover to a certain extend.

its conductance behavior even though SEM investigations do not show any visible change in the nanowire position or on the nanowire itself. This is related to the reduction of the oxygen vacancies during the plasma treatment, resulting in a reduced conductivity. The oxygen plasma treatment is only partly reversible. To reset the device conductivity, a long electroforming process of at least 1 h is necessary. However, the devices could not be brought back to the initial behavior.

Additionally, we performed conductivity measurements in air and see a current drop over two orders of magnitude (see Fig. SI 2). The current is gained back when the chamber is evacuated again. This indicates again the great impact of the oxygen vacancies on the conductivity, as oxygen ions from the atmosphere adsorb on the nanowire surface, which supports the previous suggestions.

Figure 6 shows a schematic of the expected switching process within the single $Nb_3O_7(OH)$ nanowires. The memristive switching performance is understood as accumulation/redistribution of oxygen vacancies, similar to previous studies on niobium oxide devices.[11,28] The oxygen plasma treatment study supports this assumption, as the conduction is reduced by the reduction in oxygen vacancies. Therefore, the change in the resistance during I–V cycling is related to the distribution model of oxygen vacancies, as shown in Fig. 6. The device is in a lower resistive state due to a conductive path, as shown in Fig. 6 (1). Increasing the voltage further leads to a migration of positively charged oxygen vacancies, which are repelled at the positive electrode (2) and attracted at the negative electrode. This results in a disruption of the conductive path, as well as an increased interface Schottky barrier for electrons and hence a higher resistivity. An increased Schottky barrier height, as well as the oxygen vacancy migration, during resistive switching in single metal oxide nanowires has been discussed before.[29,30] The large electric field is found to induce oxygen vacancy migration,[11] whereas for a nanowire of 2.5 μm length, oxygen vacancy accumulation at the metal interfaces has already been found as the switching process in single nanowire devices before.[30,31] A change in the polarity leads to a backward diffusion of the oxygen vacancies upon the field (3), whereas larger negative polarities (4) lead to the same but opposite effect as observed in (2).

The destructive readout process of complementary resistive switches is investigated temporally and is voltage dependent, as shown in Fig. 7. To write a specific state, either +20 or −20 V is applied to the sample for 5 s. Afterward, a readout voltage of ±12, ±10, ±8, and ±5 V is applied, with opposite polarity to the afore performed write operation. It is observed that the current for the readout process for positive readout polarities increases first, followed by a current drop. For negative, large applied potentials, the current drops quite fast, whereas for smaller potentials (<10 V), the current increases in the beginning as well, followed by a current drop. The current increase in the beginning of the readout operation is related to the polarity change induced oxygen vacancy migration similar to that illustrated in Fig. 6. For a negative write operation, the device is in condition (2) (Fig. 6). The readout operation leads to a migration of oxygen vacancies to the negative electrode and a repellence at the positive electrode, until a conductive path is formed (3). However, the oxygen vacancies are further repelled from the positive electrode, increasing the interface barrier for electrons and reducing the conductivity again (4). This process is dependent on the applied

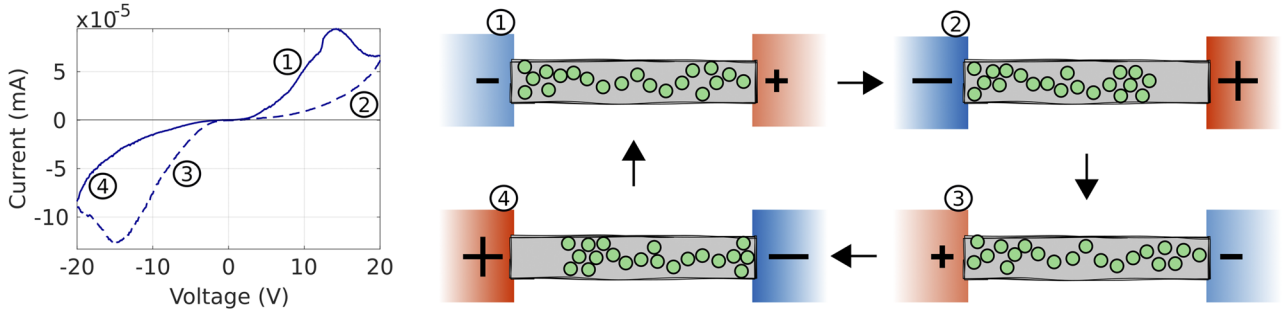

FIG. 6. CRS schematic of the single $Nb_3O_7(OH)$ nanowire devices. In (1), the device is in a LRS, which is switched to a HRS in (2) by increasing the voltage and repelling the oxygen vacancies at the positive electrode. In (3), the device switches back to the LRS due to a redistribution of the oxygen vacancies upon the opposite voltage polarity. The device is switched back to the HRS if the voltage is too large and repels the oxygen vacancies at the opposite electrode again.

potential and is slower for lower voltages. If the applied readout voltage is too small, only the high resistance state can be measured and no change in the current is observed. However, for application purposes, the readout voltage to probe the resistance state of the device is always the same. We demonstrated here that temporally resolved current–voltage measurements are a useful method for finding an appropriate readout voltage with a slow destruction of the resistance states, but a reasonable on/off ratio. Due to the asymmetric electroforming process, the destructive readout time is dependent not only on the voltage amplitude but also on the polarity for our device. A slow destruction is therefore possible for smaller positive voltages, and less energy needs to be consumed to rewrite the resistance state again.

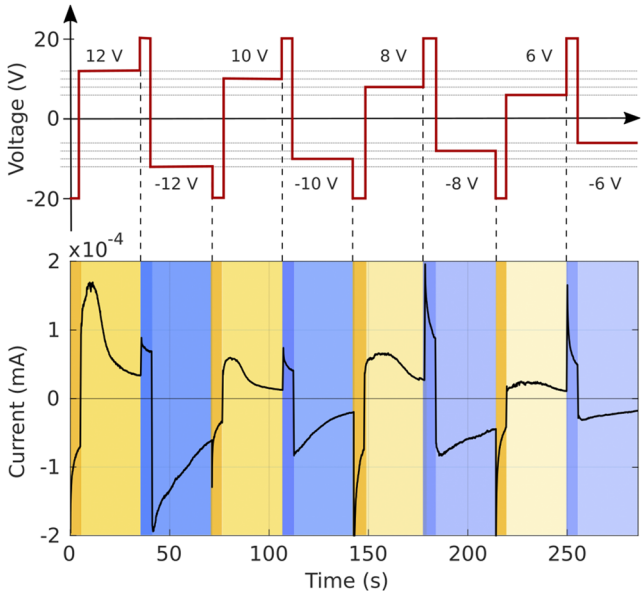

FIG. 7. The destructive readout current shows not only a voltage and time dependence but also a polarity dependence. The readout destruction process can therefore be slowed down by finding the appropriate polarity and amplitude.

IV. CONCLUSION

The growth of $Nb_3O_7(OH)$ nanowires by a hydrothermal method results in single crystalline nanowires containing planar stacking faults. 3 μm long single $Nb_3O_7(OH)$ nanowires are successfully contacted on top of two gold electrodes. The devices show a complementary resistive switching behavior, which is attributed to an oxygen vacancy migration process at the metal/hydroxide interfaces. By using an oxygen plasma treatment, the oxygen vacancy concentration is lowered, leading to a highly resistive nanowire so that switching is not possible anymore. Furthermore, the destructive readout current, which is typical for CRS cells, has been investigated in terms of voltage and time. It is shown that the destruction could be slowed down by using a positive readout polarity and low voltages.

SUPPLEMENTARY MATERIAL

See the supplementary material for the ratio calculation from EDX measurements.

ACKNOWLEDGMENTS

This work was funded by the Deutsche Forschungsgemeinschaft (DFG) under Grant Nos. SCHE 634/20-1 and SCHM 1695/14-1. Furthermore, we want to thank the group of Professor Dr. G. Hahn at the University of Konstanz for supplying SiN substrates for EDX measurements.

DATA AVAILABILITY

The data that support the findings of this study are available from the corresponding author upon reasonable request.

REFERENCES

[1] Y. B. Li, Z. R. Wang, R. Midya, Q. F. Xia, and J. J. Yang, "Review of memristor devices in neuromorphic computing: Materials sciences and device challenges," J. Phys. D: Appl. Phys. **51**(50), 503002 (2018).
[2] S. H. Jo, T. Chang, I. Ebong, B. B. Bhadviya, P. Mazumder, and W. Lu, "Nanoscale memristor device as synapse in neuromorphic systems," Nano Lett. **10**(4), 1297–1301 (2010).
[3] C. Ebenhoch and L. Schmidt-Mende, "TiO_2 nanowire array memristive devices emulating functionalities of biological synapses," Adv. Electron. Mater. **7**(2), 2000950 (2021).

[4]M. Di Ventra and Y. V. Pershin, "The parallel approach," Nat. Phys. **9**(4), 200–202 (2013).
[5]G. C. Adam, B. D. Hoskins, M. Prezioso, F. Merrikh-Bayat, B. Chakrabarti, and D. B. Strukov, "3-D memristor crossbars for analog and neuromorphic computing applications," IEEE Trans. Electron Devices **64**(1), 312–318 (2017).
[6]Z. Sun, E. Ambrosi, A. Bricalli, and D. Ielmini, "Logic computing with stateful neural networks of resistive switches," Adv. Mater. **30**(38), e1802554 (2018).
[7]G. S. Snider, "Spike-timing-dependent learning in memristive nanodevices," in *2008 IEEE International Symposium on Nanoscale Architectures* (IEEE, 2008), pp. 85–92.
[8]W. Lu and C. M. Lieber, "Nanoelectronics from the bottom up," Nat. Mater. **6**(11), 841–850 (2007).
[9]E. Linn, R. Rosezin, C. Kügeler, and R. Waser, "Complementary resistive switches for passive nanocrossbar memories," Nat. Mater. **9**(5), 403–406 (2010).
[10]Y. Yang, P. Sheridan, and W. Lu, "Complementary resistive switching in tantalum oxide-based resistive memory devices," Appl. Phys. Lett. **100**(20), 203112 (2012).
[11]X. Liu, S. M. Sadaf, S. Park, S. Kim, E. Cha, D. Lee, G.-Y. Jung, and H. Hwang, "Complementary resistive switching in niobium oxide-based resistive memory devices," IEEE Electron Device Lett. **34**(2), 235–237 (2013).
[12]J. van den Hurk, E. Linn, H. Zhang, R. Waser, and I. Valov, "Volatile resistance states in electrochemical metallization cells enabling non-destructive readout of complementary resistive switches," Nanotechnology **25**(42), 425202 (2014).
[13]S. Tappertzhofen, E. Linn, L. Nielen, R. Rosezin, F. Lentz, R. Bruchhaus, I. Valov, U. Böttger, and R. Waser, "Capacity based nondestructive readout for complementary resistive switches," Nanotechnology **22**(39), 395203 (2011).
[14]C. Ebenhoch, J. Kalb, J. Lim, T. Seewald, C. Scheu, and L. Schmidt-Mende, "Hydrothermally grown TiO_2 nanorod array memristors with volatile states," ACS Appl. Mater. Interfaces **12**(20), 23363–23369 (2020).
[15]S. B. Betzler, A. Wisnet, B. Breitbach, C. Mitterbauer, J. Weickert, L. Schmidt-Mende, and C. Scheu, "Template-free synthesis of novel, highly-ordered 3D hierarchical $Nb_3O_7(OH)$ superstructures with semiconductive and photoactive properties," J. Mater. Chem. A **2**(30), 12005 (2014).
[16]H. Zhang, Y. Wang, D. Yang, Y. Li, H. Liu, P. Liu, B. J. Wood, and H. Zhao, "Directly hydrothermal growth of single crystal $Nb_3O_7(OH)$ nanorod film for high performance dye-sensitized solar cells," Adv. Mater. **24**(12), 1598–1603 (2012).
[17]S. B. Betzler, T. Harzer, J. Ciston, U. Dahmen, G. Dehm, and C. Scheu, "Heat-induced phase transformation of three-dimensional $Nb_3O_7(OH)$ superstructures: Effect of atmosphere and electron beam," Cryst. Growth Des. **16**(8), 4309–4317 (2016).
[18]S. B. Betzler, A. L. Koh, B. V. Lotsch, R. Sinclair, and C. Scheu, "Atomic resolution observation of the oxidation of niobium oxide nanowires: Implications for renewable energy applications," ACS Appl. Nano Mater. **3**(9), 9285–9292 (2020).
[19]H. Zhang, Y. Wang, P. Liu, S. L. Chou, J. Z. Wang, H. Liu, G. Wang, and H. Zhao, "Highly ordered single crystalline nanowire array assembled three-dimensional $Nb_3O_7(OH)$ and Nb_2O_5 superstructures for energy storage and conversion applications," ACS Nano **10**(1), 507–514 (2016).
[20]W. Khan, S. B. Betzler, O. Šipr, J. Ciston, P. Blaha, C. Scheu, and J. Minar, "Theoretical and experimental study on the optoelectronic properties of $Nb_3O_7(OH)$ and Nb_2O_5 photoelectrodes," J. Phys. Chem. C **120**(41), 23329–23338 (2016).
[21]M. Hmadeh, V. Hoepfner, E. Larios, K. Liao, J. Jia, M. Jose-Yacaman, and G. A. Ozin, "New hydrogen-evolution heteronanostructured photocatalysts: Pt-$Nb_3O_7(OH)$ and Cu-$Nb_3O_7(OH)$," ChemSusChem **7**(8), 2104–2109 (2014).
[22]G. Milano, M. Luebben, Z. Ma, R. Dunin-Borkowski, L. Boarino, C. F. Pirri, R. Waser, C. Ricciardi, and I. Valov, "Self-limited single nanowire systems combining all-in-one memristive and neuromorphic functionalities," Nat. Commun. **9**(1), 5151 (2018).
[23]M. Xiao, D. Shen, M. H. Futscher, B. Ehrler, K. P. Musselman, W. W. Duley, and Y. N. Zhou, "Threshold switching in single metal-oxide nanobelt devices emulating an artificial nociceptor," Adv. Electron. Mater. **6**(1), 1900595 (2019).
[24]S. Yang, K. Hwan Ji, U. Ki Kim, C. Seong Hwang, S.-H. Ko Park, C.-S. Hwang, J. Jang, and J. Kyeong Jeong, "Suppression in the negative bias illumination instability of Zn-Sn-O transistor using oxygen plasma treatment," Appl. Phys. Lett. **99**(10), 102103 (2011).
[25]S. Gan, Y. Liang, and D. R. Baer, "Atomic control of TiO_2 (110) surface by oxygen plasma treatment," Surf. Sci. **459**(3), L498–L502 (2000).
[26]Y. Kim, B. J. Yoo, R. Vittal, Y. Lee, N.-G. Park, and K.-J. Kim, "Low-temperature oxygen plasma treatment of TiO_2 film for enhanced performance of dye-sensitized solar cells," J. Power Sources **175**(2), 914–919 (2008).
[27]X. Pan, M.-Q. Yang, X. Fu, N. Zhang, and Y.-J. Xu, "Defective TiO_2 with oxygen vacancies: Synthesis, properties and photocatalytic applications," Nanoscale **5**(9), 3601–3614 (2013).
[28]H. Maehne, H. Wylezich, S. Slesazeck, T. Mikolajick, J. Vesely, V. Klemm, and D. Rafaja, "Room temperature fabricated NbO_x/Nb_2O_5 memory switching device with threshold switching effect," in *2013 5th IEEE International Memory Workshop (IMW)* (IEEE, 2013), pp. 174–177.
[29]C. O'Kelly, J. A. Fairfield, and J. J. Boland, "A single nanoscale junction with programmable multilevel memory," ACS Nano **8**(11), 11724–11729 (2014).
[30]G. Milano, S. Porro, I. Valov, and C. Ricciardi, "Recent developments and perspectives for memristive devices based on metal oxide nanowires," Adv. Electron. Mater. **5**(9), 1800909 (2019).
[31]M. Xiao, D. Shen, K. P. Musselman, W. W. Duley, and Y. N. Zhou, "Oxygen vacancy migration/diffusion induced synaptic plasticity in a single titanate nanobelt," Nanoscale **10**(13), 6069–6079 (2018).